HHS Public Access

Author manuscript

ACS Nano. Author manuscript; available in PMC 2019 March 21.

Published in final edited form as:

ACS Nano. 2019 February 26; 13(2): 1354–1364. doi:10.1021/acsnano.8b06808.

Detection of Premalignant Gastrointestinal Lesions Using Surface-Enhanced Resonance Raman Scattering−Nanoparticle Endoscopy

Stefan Harmsen[†,‡,§,#], **Stephan Rogalla**[‡,§,#], **Ruimin Huang**[†], **Massimiliano Spaliviero**[‖], **Volker Neuschmelting**[†,⊥], **Yoku Hayakawa**[▽], **Yoomi Lee**[▽], **Yagnesh Tailor**[▽], **Ricardo Toledo-Crow**[○], **Jeon Woong Kang**[◆], **Jason M. Samii**[†], **Hazem Karabeber**[†], **Ryan M. Davis**[§], **Julie R. White**[□,△], **Matt van de Rijn**[¶], **Sanjiv S. Gambhir**[§,⊕], **Christopher H. Contag**[*,‡,▲,▼], **Timothy C. Wang**[*,▽], and **Moritz F. Kircher**[*,†,■,⬡,⬢]

[†]Department of Radiology, Memorial Sloan Kettering Cancer Center, New York, New York 10065, United States

[‡]Department of Pediatrics, Stanford University, Stanford, California 94305, United States

[§]Department of Radiology, Stanford University, Stanford, California 94305, United States

[‖]Urology Service, Department of Surgery, Sidney Kimmel Center for Prostate and Urologic Cancers, Memorial Sloan Kettering Cancer Center, New York, New York 10065, United States

[⊥]Department of Neurosurgery, University Hospital Cologne, Cologne 50937, Germany

[▽]Department of Medicine, Columbia University, New York, New York 10032, United States

[○]Research Engineering Lab, Memorial Sloan Kettering Cancer Center, New York, New York 10065, United States

[◆]Laser Biomedical Research Center, G. R. Harrison Spectroscopy Laboratory, Massachusetts Institute of Technology, Cambridge, Massachusetts 02139, United States

[□]Tri-Institutional Laboratory of Comparative Pathology, Memorial Sloan Kettering Cancer Center, The Rockefeller University, and Weill Cornell Medical College, New York, New York 10065, United States

[*]**Corresponding Authors** contagch@egr.msu.edu., tcw21@columbia.edu., moritz_kircher@dfci.harvard.edu.

[#]S. Harmsen and S. Rogalla contributed equally.

Author Contributions

S.H. designed and performed all experiments, synthesized the SERRS-NPs, and wrote the manuscript. S.R. designed and performed the dual-modality Raman endoscopy experiments and helped write the manuscript. R.H. performed immunohistochemical staining and histology correlation. M.S., V.N., J.S.M., and H.K. helped with the surgical procedures and Raman imaging of the mouse models. Y.K., Y.L., and Y.T. generated the mouse models (GAS-KO and *L2-hIL-1β*). R.T.C. built the mouse Raman endoscope and performed validation studies. J.W.K. made intellectual contributions to the mouse Raman endoscope. R.M.D. generated the 2D Raman maps and 3D cylindrical reconstructions. J.R.W. and M.vdR. performed histology and graded the lesions. C.H.C. directed the development of the circumferential Raman endoscope. C.H.C., T.C.W. and S.S.G. contributed to the experimental design, reviewed the results, provided critical support, and edited the manuscript. M.F.K. designed the experiments, directed the development of the mouse Raman endoscope, supervised the study, coordinated the researchers, and wrote the manuscript.

Notes

The authors declare the following competing financial interest(s): Stefan Harmsen and Moritz Kircher are listed as inventors on several patents related to the SERRS technology used in this work. Sanjiv Sam Gambhir and Moritz Kircher are co-founders of RIO Imaging, a startup company that aims at the clinical translation of SERRS nanoparticles.

△Cancer Biology and Genetics Program, Memorial Sloan Kettering Cancer Center, New York, New York 10065, United States

¶Department of Pathology, Stanford University, Stanford, California 94305, United States

⊕Department of Bioengineering, Department of Materials Science & Engineering, Molecular Imaging Program at Stanford, Canary Center at Stanford for Cancer Early Detection, Stanford University, Stanford, California 94305, United States

▲Department of Microbiology and Immunology, Stanford University, Stanford, California 94305, United States

▼Institute of Quantitative Health Science and Engineering, Department of Biomedical Engineering, and Department of Microbiology and Molecular Genetics, Michigan State University, East Lansing, Michigan 48824, United States

■Center for Molecular Imaging and Nanotechnology (CMINT), Memorial Sloan Kettering Cancer Center, 1275 York Avenue, New York, New York 10065, United States

⬡Department of Molecular Pharmacology, Memorial Sloan Kettering Cancer Center, 1275 York Avenue, New York, New York 10065, United States

●Department of Imaging, Dana-Farber Cancer Institute & Harvard Medical School, 450 Brookline Avenue, Boston, Massachusetts 02215, United States

Abstract

Cancers of the gastrointestinal (GI) tract are among the most frequent and most lethal cancers worldwide. An important reason for this high mortality is that early disease is typically asymptomatic, and patients often present with advanced, incurable disease. Even in high-risk patients who routinely undergo endoscopic screening, lesions can be missed due to their small size or subtle appearance. Thus, current imaging approaches lack the sensitivity and specificity to accurately detect incipient GI tract cancers. Here we report our finding that a single dose of a high-sensitivity surface-enhanced resonance Raman scattering nanoparticle (SERRS-NP) enables reliable detection of precancerous GI lesions in animal models that closely mimic disease development in humans. Some of these animal models have not been used previously to evaluate imaging probes for early cancer detection. The studies were performed using a commercial Raman imaging system, a newly developed mouse Raman endoscope, and finally a clinically applicable Raman endoscope for larger animal studies. We show that this SERRS-NP-based approach enables robust detection of small, premalignant lesions in animal models that faithfully recapitulate human esophageal, gastric, and colorectal tumorigenesis. This method holds promise for much earlier detection of GI cancers than currently possible and could lead therefore to marked reduction of morbidity and mortality of these tumor types.

Graphical Abstract

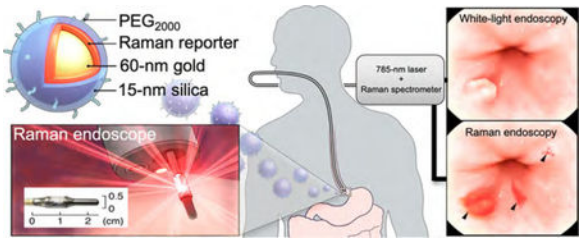

Keywords

early detection; cancer; Raman; nanoparticle; endoscopy; preclinical

Timely and accurate diagnosis of incipient gastrointestinal (GI) cancers is critical. It has been shown that early detection of asymptomatic disease of the GI tract improves the chances of curative intervention by 50−80% as compared to the poor five-year survival rates for symptomatic advanced malignant disease.[1–4] Especially in high-risk patients who already undergo periodic white light endoscopic surveillance, it is estimated that about three times more dysplastic lesions—the most clinically relevant lesions to predict malignant progression—are missed relative to healthy individuals.[5–8] The reasons for this high miss rate are the subtle appearance of such lesions and sampling errors inherent to a random-biopsy surveillance paradigm. Further, endoscopic assessment and diagnosis of GI tract lesions are operator-dependent and prone to subjectivity, which increases interobserver variability and thus further compromises diagnostic accuracy.[9] Lastly, surveillance for gastric and colorectal lesions can be challenging due to the large surface areas that need to be surveyed, poor intestinal cleansing, and the need to perform the procedure in a reasonable period of time. Moreover, even when disease is detected, it is often difficult to determine the true extent of the lesion, thus impeding the ability to achieve complete resection or ablation using minimally invasive (endo-) therapeutic intervention. Consequently, approximately 33% of GI tract lesions recur at or near the therapeutic site,[10–12] commonly requiring more aggressive yet often noncurative (systemic) treatments that negatively impact the patients' quality of life. There is a clear unmet need for sensitive and specific imaging approaches that enable detection of neoplastic lesions in the GI tract, ideally at a premalignant stage before invasive cancers develop (Figure 1a).

Intrinsic Raman endoscopy, which probes compositional differences between tissues, is currently being clinically explored to distinguish normal from premalignant and malignant GI tract lesions. While this intrinsic approach does enable the differentiation between the different tissue types, it has many inherent limitations, such as the required long acquisition times, that currently prevent its clinical implementation as a comprehensive endoscopic imaging approach.[13,14] On the other hand, we recently demonstrated that contrast-enhanced Raman imaging using surface-enhanced resonance Raman scattering nanoparticles (SERRS-NPs) provides femtomolar sensitivity *in vivo* as a result of the unparalleled signal specificity of SERRS-NPs' Raman spectral "fingerprint", which is virtually nonexistent in biological tissues.[15,16] In fact, we demonstrated that as a result of the high sensitivity of the SERRS-NPs combined with passive, but selective accumulation due to increased permeability of the immature tumor vasculature (as illustrated in Figure 1b), we were able to detect and

delineate a wide variety of cancer types in preclinical carcinogenesis models.[16–18] Moreover, in the same study, we noted that the SERRS-NPs also sporadically enabled the detection of premalignant precursor lesions of prostate and pancreatic cancers.[16]

With the aim of detecting incipient GI tract cancers and to facilitate targeted biopsies and improve therapeutic intervention, in the current study we systematically assessed whether (1) SERRS-NPs (at the current dose) could enable detection of premalignant GI lesions of the esophagus, stomach, and intestines and (2) whether the SERRS-NPs sufficiently accumulate in these premalignant precursor lesions to provide the sensitivity needed for detection or imaging of such lesions using a custom-built small-animal Raman endoscope and a clinically applied Raman endoscope.[19,20] We demonstrated that SERRS-NPs indeed enable real-time detection and delineation of premalignant dysplastic GI tract lesions—the clinically most significant precursor lesion—in mouse models of esophageal, stomach, and colorectal carcinogenesis. Furthermore, we demonstrate that as a result of the accumulation of these highly sensitive SERRS-NPs at these lesions following intravenous administration, the use of a spectral Raman endoscope to pinpoint and guide biopsy toward dysplastic lesions at the gastroesophageal junction is feasible. Finally, we show *in vivo* in a genetic rat model of colorectal carcinogenesis that SERRS-NP Raman endoscopy using a clinically applied circumferentially scanning miniature Raman endoscope enabled the simultaneous real-time acquisition of Raman imaging and conventional white-light endoscopy, allowing sensitive, Raman-based tumor detection while preserving the macroscopic tissue context provided by the white-light endoscopy. As such, SERRS-NP Raman endoscopy could become a valuable adjunct to white-light endoscopy to improve endoscopic detection of premalignant GI tract lesions (Figure 1c,d).

RESULTS AND DISCUSSION

Characterization of SERRS-NPs.

SERRS-NPs were synthesized through rapid silica encapsulation of dialyzed citrate-capped 60 nm gold nanoparticles in the presence of a near-infrared dye, IR780 perchlorate, which has a maximum absorption at 780 nm. Since we use a 785 nm excitation laser in our Raman microscopy and endoscopy systems, the electronic transition of the near-infrared absorbing Raman reporter of the SERRS-NP is close to or in resonance with the excitation laser to provide an additional enhancement factor of 10^2–10^6 *versus* surface-enhanced Raman scattering nanoparticles that use nonresonant dyes. Consequently, while nonresonant SERS nanoparticles demonstrate detection limits in the low picomolar range (10^{-12} M),[21] resonant SERRS-NPs can achieve 1000-fold lower limits of detection in the low-femtomolar/attomolar range (10^{-15}–10^{-17} M) under the same imaging conditions (Figure S1).[15,16]

After modification of the silica surface with a thiol functionality, the surface of the SERRS-NPs was passivated with methoxy-terminated polyethylene glycol (PEG; 2 kDa) using straightforward maleimide chemistry. The PEGylated SERRS-NP were narrowly dispersed with a hydrodynamic diameter of ~110 nm and a signal intensity of ~35 000 counts for the 950 cm^{-1} diagnostic peak of the PEGylated SERRS-NP (Figure 2).

Route of Administration and Distribution of SERRS-NPs in the Gastrointestinal Tract.

The ability of our SERRS-NPs to enable detection of incipient cancers without the need for modification with a targeting moiety (*e.g.*, antibody, peptide, *etc.*) that would require *a priori* knowledge of molecular markers was evaluated in clinically relevant animal models of Barrett's esophagus/esophageal, gastric, and colorectal tumorigenesis. Since oral or topical administration did not seem to be a viable route of administration due to nonspecific mucosal adhesion of orally administered SERRS-NPs (Supplementary Figure S2), all studies were performed by intravenously (i.v.) injecting the SERRS-NPs *via* the tail vein at a dose of 30 fmol/g (injection volume of 150 μL of 3.5 nM SERRS-NPs, which is equivalent to ~500 fmol injected nanoparticles per mouse). Furthermore, we assessed the distribution of intravenously administrated SERRS-NPs *in situ* and in normal tissues of the upper GI tract of healthy control mice and found no nonspecific accumulation of SERRS-NPs at the gastroesophageal junction (GEJ), in the stomach, or in the intestines ($n = 4$; Supplementary Figure S3a−c).

Detection of Premalignant Lesions of the Esophagus.

Bile acid (BA)-treated transgenic human interleukin-1β (*L2-hIL-1β*) mice develop esophagitis, Barrett-like metaplasia, and esophageal adenocarcinoma through the metaplasia −dysplasia−adenocarcinoma sequence.[22] As such, this model faithfully recapitulates the development of Barrett's esophagus and esophageal adenocarcinoma in humans. BA-treated 12−18-month-old *L2-hIL-1β* animals ($n = 5$) were tail-vein injected with SERRS-NPs, and Raman imaging was performed 18 h later. As shown in Figure 3a,b, the nontargeted SERRS-NPs enabled Raman-based detection of dysplastic lesions at the GEJ, which is precisely where the major histopathological changes occur in this particular model,[22] as well as in human patients.[23] Immunohistochemistry was performed on the SERRS-positive lesions to stain for the stemness marker CD44, proliferation marker MKI67, and the SERRS nanoparticle PEG-polymer coating. While in normal tissue CD44 expression at the GEJ is restricted to the proliferative basal region of the epithelium (Supplementary Figure S3b,c), the SERRS-positive lesions at the GEJ of BA-treated *L2-hIL-1β* animals demonstrated diffuse expression of CD44, which corresponds to CD44 expression patterns found in Barrett's associated dysplasia of the intestinal subtype.[24] Further, in contrast to normal GEJ tissue, MKI67 is also diffusely expressed throughout the SERRS-positive lesion (Figure 3c) and no longer restricted to the proliferative basal region of the GEJ. Lastly, anti-PEG immunostaining was used to stain for the polymer that is conjugated to the SERRS nanoparticle surface. The positive granular anti-PEG stain confirms the presence of the SERRS-NPs in the indicated lesion.

Detection of Premalignant Lesions of the Stomach.

In *Helicobacter felis*-infected gastrin-knockout (GAS-KO) mice cotreated with the carcinogen *N*-methyl-*N*-nitrosourea (MNU), dysplasia and/or adenocarcinoma typically develops at the pyloric antrum,[25] which closely recapitulates *H. pylori*-induced gastric tumorigenesis in humans. Following intravenous injection of SERRS-NPs (30 fmol/g) in the MNU-treated GAS-KO mice ($n = 5$), several SERRS-positive lesions were detected at the pyloric antrum (Figure 4a). Histopathological examination confirmed the dysplastic nature

of these SERRS-positive antral lesions (Figure 4a−c), which exhibited diffuse CD44 and MKI67 expression relative to CD44 and MKI67 expression patterns in a SERRS-negative control region within the same organ (Supplementary Figure S4a−c). The selectivity of the SERRS-NPs for incipient gastric cancer detection is further corroborated by PEG immunostaining, which was positive in the SERRS-positive dysplastic antral lesions and negative in SERRS-negative normal tissue in the same diseased stomach (Figure 4c and Supplementary Figure S4c).

Detection of Premalignant Lesions of the Intestines.

$Apc^{Min/+}$ mice harbor a chemically induced mutation in the *Apc* gene resulting in a premature truncation of its gene product, which predisposes these animals to the formation of intestinal adenoma formation.[26] Raman imaging was performed *in vivo* on exteriorized ileal segments of symptomatic $Apc^{Min/+}$ mice ($n = 5$) injected with SERRS-NPs (30 fmol/g) 18 h prior to imaging. As shown in Figure 5a and Supplementary Figure S5, multiple discrete SERRS-positive lesions were detected that were shown to correspond to the presence of adenomatous polyps based on H&E and cyclin D1 (CCND1)-immunostaining. Cyclin D1 (CCND1) was used as a marker, since its nuclear overexpression is found in intestinal lesions of $Apc^{Min/+}$ mice due to abnormal β-catenin translocation resulting from the *Apc* gene mutation.[27] To further corroborate the performance of the SERRS-NPs, *ex vivo* Raman imaging was performed on intact intestinal tracts of $Apc^{Min/+}$ mice ($n = 5$). It was shown that SERRS-NP augmented Raman imaging enabled accurate delineation of lesions as small as 500 μm (Supplementary Figure S6). Immunostaining for cyclin D1 (CCND1) and PEG was performed on the SERRS-positive intestinal sections. Of note, in an asymptomatic animal that had to be sacrificed because of a large mammary tumor, which is known to arise in this model,[28] a small SERRS-positive lesion was found in the intestinal tract following intravenous SERRS nanoparticle injection. This lesion was identified as an adenomatous polyp by histopathological examination (Supplementary Figure S6).

Next, we assessed the sensitivity and positive predictive value (*i.e.*, precision) of SERRS-based Raman imaging for the detection of (pre-) malignant lesions of the intestinal tract in $Apc^{Min/+}$ mice ($n = 4$). The intestines proximal to the cecum of SERRS-NP-injected $Apc^{Min/+}$ mice were scanned with Raman imaging and subsequently embedded in paraffin. Then, the SERRS-positive lesions in each intestinal tract were counted and carefully matched to histology (Figure 5b). On average, 33 SERRS-positive lesions were counted in the scanned tissues, of which ~23 could be matched to histology. This discrepancy is related to the sectioning of the tissue, which can result in loss of lesions due to the fact that certain lesions are located outside of the sectioning plane. We therefore only included the number of SERRS-positive lesions that could be matched to histology in the analysis and found a sensitivity of 93.1% and a positive predictive value (or precision) of 89% (Table 1). We also assessed how including the SERRS-positive lesions that could not be correlated by H&E affected the positive predictive value. By assuming either a 0% or 100% match on histology, the value of the positive predictive value was determined to lie within 83−93%. The few detected false positives were identified as gut-associated lymphoid tissue (GALT), which could be easily discriminated from intestinal dysplasia or adenocarcinoma during a clinical

endoscopic procedure *via* the white-light endoscopy imaging and thus are expected to only affect the accuracy in our mouse model studies (Supplementary Figure S7).

Feasibility of Endoscopic Detection of Premalignant Upper and Lower GI Lesions in Mice Using a Custom-Built Small-Animal Raman Endoscope.

In order to test the feasibility of endoscopic detection in mouse models, we first designed and built a small-animal spectral Raman endoscope consisting of a 550 μm diameter optical fiber that was connected to a Raman spectrometer (Figure 6a; see also Supplementary Figure S8 and Methods). Using this custom-built endoscope, we performed *ex vivo* endoscopic surveillance of the GI tract. Figure 6d shows an example of the detection of dysplasia at the GEJ of *L2-hIL-1β* mice. The diagnostic 950 cm^{-1} band of the SERRS-NPs was found to be associated with premalignant lesions at the GEJ. In $Apc^{Min/+}$ mice, we exteriorized the intestinal tract, inserted the Raman endoscope proximal to the cecum, and slowly advanced the endoscope along the ileum. This allowed us to carefully maneuver the endoscope and, more importantly, also enabled us to precisely locate and resect a lesion where the diagnostic 950 cm^{-1} band of the SERRS-NPs was detected (Figure 6e). Histopathological examination identified the resected SERRS-positive lesions as dysplastic intestinal adenomas.

Toward Clinical Translation: Feasibility of Detecting Premalignant GI Lesions Using a Clinical Grade, Dual-Modality, Raman/White-Light Endoscope.

While we were able to visualize the spectra of SERRS-NPs using the above approach in mice, the ultimate goal toward clinical translation is to acquire circumferential Raman images of the entire intestinal lumen and to combine this with conventional white-light endoscopic imaging. We therefore employed our dual-modality white-light/Raman clinical grade endoscopic imaging system in conjunction with the i.v.-injected SERRS-NPs in a larger animal (rat) model.[19] This system consists of a clinically approved white-light endoscope and a clinically validated, first-in-human, noncontact circumferentially scanning Raman endoscope.[19] The system was inserted rectally at a depth of 8 cm in the colons of $Apc^{Pirc/+}$ rats ($n = 5$)—a model that closely recapitulates human colorectal tumorigenesis—that received PEGylated SERRS-NPs 18 h prior to *in vivo* endoscopic Raman imaging. The dual-modality endoscopic imaging system was retracted at a constant speed (160 mm/min) while circumferentially scanning the whole colorectal luminal surface (100 pixels/rotation at 1 Hz), thus generating Raman maps in real time. The white-light video provided the relevant anatomical context (Figure 7b); the presence of SERRS signal was associated with colorectal polyps (Figure 7b,c; 1), while lack of SERRS signal was associated with normal appearance of the colonic surface (Figure 7b,c; 2). A three-dimensional cylindrical projection (Figure 7d) of the two-dimensional Raman map (Figure 7c) demonstrated excellent correlation between the Raman imaging and presence of polyps in the colon (Figure 7e). Histopathologic examination of the SERRS-positive lesions (Figure 7e,f; 1, 3) confirmed by veterinarian pathologists proved the presence of adenomatous polyps. Furthermore, lack of SERRS signal (Figure 7c,d; 2) correlated with normal appearance of the colorectal tissue (Figure 7f, 2).

Here we demonstrate the ability of contrast-enhanced Raman imaging using SERRS-NPs to detect incipient cancers along the entire GI tract. We show that PEGylated SERRS-

NPs—not requiring a specific targeting moiety—home to incipient GI tract cancers of the esophagus, stomach, and intestines. In addition to a genetic mouse model of intestinal polyps, we also tested $Apc^{Pirc/+}$ rats, which closely recapitulate colorectal tumorigenesis in humans.[22,25,29,30] It is important to note that these models have distinct molecular mechanisms that underlie tumorigenesis, and thus a single, targeted molecular imaging agent would be unlikely to detect neoplastic lesions in all regions of the GI tract. By relying on a pathophysiological mechanism common to all cancer types, the enhanced permeability and retention (EPR) effect, we have demonstrated robust detection of very small premalignant lesions in multiple regions of the GI tract. Maeda *et al.* have shown that the EPR effect exists in virtually all tumor types and is highly specific for tumors.[31,32] In infection or inflammation, only enhanced permeability exists, but not enhanced retention. The retention is largely attributed to abnormalities in the draining lymphatic vessels, which remain relatively intact in infection or inflammation.[31,32] Hagendoorn *et al.* showed that the vascular changes governing EPR such as altered vascular permeability and nonfunctional lymphatic vessels already occur during the early stages of carcinogenesis.[33] It is likely that the small size of these lesions limits the number of accumulated particles, and, therefore, extremely sensitive detection methods are needed. The fact that we were able to visualize such small lesions that had not even progressed yet to invasive cancers indicates that the arterial capillaries supplying these preneoplastic lesions likely already had developed features of neovasculature such as fenestrations large enough to allow extravasation of our SERRS-NPs from the capillary bed into the parenchymal cells of the lesion. We conclude that our successful imaging was enabled by the extraordinary sensitivity of our SERRS-NPs, whose limit of detection is in the low femtomolar (10^{-15} M) range.

In contrast, most fluorescent-based molecular imaging agents, including quantum dots, need to achieve a local concentration in the nanomolar (10^{-9} M) range in order to be detectable *in vivo*.[34] This approximately 1 million-fold higher sensitivity can explain why SERRS-NPs are (1) able to detect such previously occult lesions and (2) can do so in a universal fashion in the GI tract, independent of the tumor type (esophageal, gastric, colonic).

In this study, we demonstrate highly sensitive SERRS-NP-based lesion detection with three different methods: (1) conventional two-dimensional imaging of GI organs using an InVia Raman imaging system; (2) spectroscopic detection of lesions using a custom-built mouse Raman endoscope; and (3) combined Raman/white-light imaging using a recently developed clinical Raman endoscope.[19] This circumferential Raman endoscope was designed to fit into the small instrument channel of the colonoscopes that are routinely used in patients.[19] Cancer detection benefits from multimodality approaches, and therefore we used a clinical white-light endoscope to evaluate anatomic abnormalities, a Raman endoscope to detect intravenously injected SERRS-NPs, and conventional histopathologic approaches to validate the *in vivo* imaging. We chose the $Apc^{Pirc/+}$ rat model for these studies, because these animals are large enough to accommodate the clinical endoscopes, and it is an established, genetically engineered model that mimics the known stepwise development of colonic cancer from the initial development of premalignant polyps. The direct side-by-side comparison of the traditional white-light endoscopy and the SERRS-NP-augmented Raman imaging reveals the potential for Raman screening in the GI tract. We were able to detect premalignant lesions using SERRS-NP imaging that were not always visible with white-

light endoscopy. The white-light provided the relevant anatomical context when SERRS signal was detected, an ability that will greatly facilitate Raman-guided biopsy or (endo-) therapeutic intervention in humans in the future.

In contrast to intravenous administration of SERRS-NPs, several groups evaluated topical administration of nanoparticles for detection of GI tract lesions. In a recent study by Kim *et al.* (2017), it was shown that orthotopically implanted human colorectal cancer cell lines that overexpress epidermal growth factor receptor (EGFR) and vascular endothelial growth factor (VEGF) could be endoscopically detected and visualized using EGFR- and VEGF-targeted SERS nanoparticles.[35] Interestingly, in a study by Liu *et al.* it was demonstrated that topical application of SERS nanoparticles for endoscopic detection of GI tract lesions is only feasible when a ratiometric method is used that corrects for nonspecific binding of the nanoparticles to the mucosa lining the luminal surfaces of the GI tract.[36] A cocktail of HER2, EGFR, and nontargeted SERS nanoparticles with distinct Raman fingerprints was topically applied to the esophagus of a rat that was orthotopically implanted with EGFR-and HER2-overexpressing cell lines. Multiplexed Raman imaging was performed, and Raman maps were generated based on ratiometric quantification of targeted *versus* nontargeted SERS nanoparticles, which provided unambiguous visualization of biomarker-positive lesions. A limitation of both proof-of-principle studies using targeted nanoparticles is that to enable comprehensive disease detection the selected biomarker(s) should be ubiquitously (over)expressed in the lesions. However, the genomic landscape of GI tract tumors, even that of premalignant lesions, shows a large degree of intra- and intertumoral heterogeneity.[29,37] Consequently, approaches involving targeted SERS nanoparticles may lead to an increase in false negatives (*i.e.*, miss rate) relative to strategies involving systemically administered nontargeted SERRS nanoparticles. Furthermore, topically applied targeted nanoparticles will only bind to the luminal surface of a lesion, whereas systemically administered SERRS nanoparticles will accumulate throughout the lesion, allowing not only detection in a screening scenario but also Raman-guided resection, and potentially photothermal ablation, when therapeutic intervention is required. At least for colorectal cancers, there are also promising stool DNA tests being developed that can potentially diagnose the presence of adenomas and carcinomas in an elegant fashion;[38,39] however localization of such lesions with endoscopy will still be necessary. Here, our approach and stool DNA tests could work together synergistically.

While we demonstrated that the nontargeted SERRS-NPs uniformly accumulate in premalignant tumors of the GI tract in clinically relevant animal models enabling early endoscopic detection and guidance of (endo-) therapeutic intervention, we recognize that following intravenous administration, the SERRS nanoparticles will accumulate mostly in the liver and spleen, where the silica shell will biodegrade within several days postaccumulation, leaving behind the gold nanocore, which is metabolically inert. Consequently, no long-term toxicities are expected from the residual gold nanocores. In fact, several studies with systemically administrated gold/silica hybrid nanoparticles (AuroLase; size ~150 nm) or rhTNF-coated gold nanoparticles (size ~30 nm) in humans have so far not reported any adverse events or toxicities related to the systemic administration or retention of gold nanoparticles.[40,41] Surely, while extensive long-term toxicity studies will have to be

performed in larger animal models before SERRS-NPs can be translated to the clinic, the Raman endoscope has already been translated to humans.[19]

CONCLUSION

We demonstrated the potential of contrast-enhanced Raman endoscopy for highly sensitive detection of precursor lesions of GI tract cancers in clinically relevant transgenic animal models that closely recapitulate human tumorigenesis in high-risk patients that have predisposing conditions such as Barrett's esophagus, *H. pylori* infection, or familial adenomatous polyposis. Since the composition of SERRS-NPs is biocompatible and the real-time dual-modal Raman endoscopy system has already been clinically validated in humans, there is a viable path toward clinical translation. In the future, contrast-enhanced Raman endoscopy could become an adjunct to conventional white-light endoscopic surveillance to enhance detection and guide (endo-) therapeutic intervention of precursor lesions of GI tract cancers to ultimately enable cancer prevention.

METHODS

All chemicals were obtained from Sigma-Aldrich (St. Louis, MO, USA) and used as received unless otherwise noted.

Surface-Enhanced Resonance Raman Scattering Nanoparticle Synthesis.

The PEGylated SERRS-NPs were synthesized by rapidly adding 7.5 mL of 1% (w/v) sodium citrate tribasic dehydrate to 1.0 L of a boiling aqueous solution of 20 mM gold chloride. The as-synthesized 60 nm gold nanoparticles were collected by centrifugation and dialyzed (Slide-a-lyzer G2; MWCO: 3.5 kDa; Thermo Fisher Scientific, Inc. Waltham, MA, USA). The dialyzed 60 nm gold nanoparticles were encapsulated in resonant Raman reporter (IR780 perchlorate)-embedded silica *via* a modified Stöber procedure, yielding the SERRS nanoparticle as previously described.[42] In brief, a solution containing 9.0 mL of 2-propanol, 1.2 mL of tetraethoxyorthosilicate (TEOS; 99.999% v/v), and 75 μL of 25 mM IR780 perchlorate (or 75 μL of 25 mM IR792 perchlorate; "flavor 2") in dimethylformamide was rapidly added to a dispersion of 4.5 mL of 2.0 nM 60 nm gold nanoparticles in 30 mL of 2-propanol containing 600 μL of ammonium hydroxide (28% v/v). After stirring for 15 min at 500 rpm, the SERRS nanoparticles were collected using centrifugation (10500*g*). The SERRS nanoparticles were washed 3× with ethanol and redispersed in 1.0 mL of ethanol. The surface of the SERRS nanoparticle was functionalized with a 5% (v/v) (3-mercaptopropyl)trimethoxysilane (MPTMS) in 90% (v/v) ethanol (90 min at 70 °C) in order to conjugate monofunctional 2 kDa methoxy-terminated PEG (1% w/v) to the nanoparticle *via* straightforward maleimide chemistry (90 min at ambient conditions in 10 mM 2-(*N*-morpholino)ethanesulfonic acid (MES) pH 7.1). Following PEG conjugation, the PEGylated SERRS nanoparticles were washed 3× with water and redispersed in an appropriate volume of water to yield a 7.0 nM dispersion of PEGylated SERRS-NPs. Before intravenous injection, 80 μL of 7.0 nM PEGylated SERRS-NPs in water was dispersed in an equal volume of 0.22 μm filter-sterilized 20 mM MES buffer (pH 7.3) to yield 3.5 nM PEGylated SERRS-NP in 10 mM MES buffer.

PEGylated SERRS Nanoparticle Characterization.

The as-synthesized PEGylated SERRS nanoparticles (7.0 nM in water) were characterized using transmission electron microscopy (TEM), nanoparticle tracking analysis (NTA; NS500, Malvern), and Raman spectroscopy. TEM and NTA were used to determine the size and hydrodynamic diameter of the PEGylated SERRS-NPs, respectively. In brief, 1.0 μL of 1.0 nM PEGylated SERRS-NPs was dropped on a carbon-coated copper TEM grid (CF300-Cu; Electron Microscopy Sciences), air-dried, and analyzed using a magnification of 100 000× on a JEOL 1200-EX II transmission electron microscope operating at 80 kV. For hydrodynamic diameter and concentration measurements, a 1.0 mL sample containing PEGylated SERRS-NPs (1000× diluted in water) was analyzed on an NTA. Finally, Raman spectroscopy was performed on 10 μL of a 1.0 nM PEGylated SERRS-NP dispersion in a white 1536-well plate using a 785 nm laser operating at 50 μW and an acquisition time of 1.0 s.

Animals Models.

All animal experiments were approved by the Institutional Animal Care and Use Committees of Memorial Sloan Kettering Cancer Center (#06–07-011), Columbia University Medical Center (#AAAF2657), and Stanford University (#27715). All applicable institutional guidelines for the care and use of animals were followed.

Chronic Esophagitis Mouse Model (L2-hIL-1β).—The *L2-hIL-1β* mice were generated as previously described.[22] Briefly, mice were generated by targeting expression of hIL-1β to the esophagus using the Epstein−Barr virus promoter (ED-L2). The human *IL-1β* cDNA consisted of a constitutively secreted form (*i.e.*, not requiring caspase-1 cleavage) of mature human *IL-1β* cDNA fused with the signal sequence derived from the structurally related human *IL1-RA*. Female *L2-hIL-1β* mice were placed on drinking water containing bile acids (0.3% deoxycholic acid, pH 7.0) at the age of three months.

Helicobacter-Induced Gastric Cancer Mouse Model.—Eight to 12-week old gastrin-knockout (GAS-KO) male mice in a C57BL/6 background were infected by oral gavage with *H. felis* in 0.2 mL of trypticase broth three times per week on every other day for a total dose of 100 million colony-forming units per mouse. MNU was dissolved in distilled water at a concentration of 240 ppm and freshly prepared three times per week for administration in drinking water in light-shielded bottles *ad libitum*. Mice were given drinking water containing 240 ppm MNU on alternate weeks for a total of 10 weeks (total exposure of 5 weeks). MNU was administered 2 weeks after *H. felis* inoculation as described previously.[25]

Intestinal Tumorigenesis Mouse Model ($Apc^{Min/+}$).—Heterozygous C57BL/6J-*Apc*^{Min} ($Apc^{Min/+}$) female mice were obtained from The Jackson Laboratory (Bar Harbor, ME, USA) and were raised on a high-fat diet.

Colorectal Tumorigenesis Rat Model ($Apc^{Pirc/+}$).—Heterozygous $Apc^{Pirc/+}$ rats 12 to 16 weeks old were obtained from Professor James Amos-Landgraf, Department of Veterinary Pathobiology, University of Missouri (Columbia, MO, USA).

Raman Imaging.

Bile-acid-treated 12−18-month-old *L2-hIL-1β* ($n = 5$), 10-month-old *H. felis*/MNU-treated gastrin (GAS-KO) mice ($n = 5$), and $Apc^{Min/+}$ mice ($n = 8$) were tail-vein injected with the PEGylated SERRS-NPs (30 fmol/g) in 10 mM MES buffer. The *L2-hIL-1β* and GAS-KO animals were sacrificed *via* CO_2 asphyxiation the next day, and their organs scanned by Raman imaging *ex vivo*. Symptomatic >5-month old $Apc^{Min/+}$ mice were anesthetized ($n = 5$; isoflurane). A mini-laparotomy was performed, and a small loop of the ileum was exteriorized and surveyed by Raman imaging for SERRS-positive lesions (10 mW laser power, 1.5 s acquisition time, and 5× objective). The sutures were left in place for later retrieval and proper orientation of the loop. The tissues were placed back into the intraperitoneal cavity, and the incision was closed in layers. After 8 h, the animal was sacrificed by CO_2 asphyxiation and the marked area was recovered and fixed in 4% paraformaldehyde. All *in vivo* and *ex vivo* Raman imaging of the tissues was performed on an InVia Raman microscopy system equipped with a 1-in. charge-coupled device detector with a spectral resolution of 1.07 cm^{-1} and a 785 nm diode laser (Renishaw Inc., Hoffman Estates, IL, USA). Typically, the tissues were raster scanned using a 10 mW laser power, a 1.5 s acquisition time, and a 5× objective. Raman images were generated by applying a direct classical least-squares algorithm (Wire 3.4 software, Renishaw), which linearly matches the predefined Raman spectrum of the SERRS-NPs with the Raman spectra of the scanned tissues.

Custom-Built Miniature Mouse Raman Endoscope.

For endoscopic acquisition of SERRS-NP signal in the mouse models, we built a small-animal Raman endoscope. It consists of a 550 μm diameter multimode optical fiber (FG550LEC, Thorlabs Inc., Newton, NJ, USA) that was directly coupled to a hand-held spectroscopic probe (BAC100 B&WTek Inc., Newark, DE, USA) by replacing the metallic shaft lens-housing unit with a fiber FC/PC interface (PAF-X-2-B, Thorlabs). The probe was connected to a Raman spectrometer (MiniRam, B&WTek Inc.). All Raman endoscopy was performed with a 785 nm diode laser operating at 50 mW laser power using an acquisition time of 100 ms. The optical fiber used was of low hydroxyl content but still produced a measurable stimulated Raman scattering background. Before endoscopic surveillance, a background Raman spectrum was collected of the optical fiber, which was subsequently subtracted in real time from the Raman spectra obtained during endoscopic tissue surveillance.

Contrast-Enhanced Raman Endoscopy in Mice.

The procedure for Raman endoscopic surveillance was as follows: $Apc^{Min/+}$ ($n = 5$) or *L2-hIL-1β* ($n = 3$) mice injected with PEGylated SERRS-NPs (30 fmol/g) were sacrificed by CO_2 asphyxiation the next day. The intestines of $Apc^{Min/+}$ mice were exteriorized, and the Raman endoscope was carefully inserted into the small intestine proximally to the cecum and slowly advanced along the small intestine. In the *L2-hIL-1β* mice, Raman endoscopy was performed on the upper GI tract (*i.e.*, esophagus and stomach) *ex vivo* by slowly advancing the optical fiber along the esophagus toward the stomach. When SERRS

nanoparticle signal was detected, the tissue was sectioned and processed for histological examination.

Combined Real-Time Contrast-Enhanced Raman and White-Light Endoscopy in $Apc^{Pirc/+}$ Rats.

After polyps were detected in the $Apc^{Pirc/+}$ rats ($n = 5$) by white-light endoscopy, we injected PEGylated SERRS-NPs intravenously *via* tail vein into the rats at a dose of 30 fmol/g. The next day, the rats were anesthetized using isoflurane, and their colons rinsed with phosphate-buffered saline and the mucolytic agent acetylcysteine. Concomitant white-light and real-time Raman endoscopic imaging was performed using a white-light endoscope (Pentax EPK-1000) that was coupled to a custom-built circumferentially scanning Raman endoscope equipped with a 785 nm laser.[20] The dual-modal white-light/Raman endoscope was inserted rectally approximately 8 cm deep into the colon of the anesthetized rat, and the colon was scanned in real time during retraction at a constant speed (160 mm/min). Following endoscopic surveillance, the rats were sacrificed, and the colons were removed, fixed in formalin, and processed for histopathological examination by a pathologist blinded to the endoscopic Raman imaging results.

Histology and Immunohistochemistry.

After Raman imaging, the tissues were fixed in 4% paraformaldehyde (4 °C overnight) and subsequently processed to be embedded in paraffin. Tissue sections (5 μm) were stained with hematoxylin and eosin (H&E), and immunohistochemistry staining was performed using the DISCOVERY XT biomarker platform (Ventana, Tucson, AZ, USA). Heat-induced epitope retrieval was performed using citrate buffer (pH 6.0). The primary antibodies were diluted as follows: anti-CD44 antibody (1:500; #550538; BD Biosciences, San Jose, CA, USA), anti-Ki-67 antibody (1:250, VP-RM04, Vector Laboratories Inc., Burlingame, CA, USA), anti-CCND1 antibody (1:500; Abcam, Cambridge, MA, USA), and anti-PEG antibody (1:100, PEG-B-47, ab51257, Abcam). All biotin-labeled secondary antibodies, including anti-rabbit antibody (1:300, BA-1000) and anti-rat antibody (1:300, BA-9400), were purchased from Vector Laboratories. All murine specimens were examined by a veterinary pathologist (JRW) from the Tri-Institutional Laboratory of Comparative Pathology who was blinded to the Raman images. All rat specimens were examined by a pathologist (MvdR) from the Department of Pathology at Stanford University who was blinded to the Raman images.

Supplementary Material

Refer to Web version on PubMed Central for supplementary material.

ACKNOWLEDGMENTS

The authors would like to thank the Electron Microscopy and Molecular Cytology Core Facility at Memorial Sloan Kettering Cancer Center (MSKCC) for technical assistance. We thank Matthew A. Wall (MSKCC) for insightful discussions. This work was supported in part by the following grants (to M.F.K.): NIH R01 EB017748, R01 CA222836, and K08CA16396; Damon Runyon-Rachleff Innovation Award (DRR-29–14), Pershing Square Sohn Prize by the Pershing Square Sohn Cancer Research Alliance, MSKCC Center for Molecular Imaging and Nanotechnology Grant, Technology Development Grant, Center for Molecular Imaging and Nanotechnology (CMINT) Grant, Experimental Therapeutics Grant, and Molecularly Targeted Intra-Operative Imaging Grant, Geoffrey Beene Cancer Research Center at MSKCC Grant Award, and Shared Resources Award. We also

acknowledge the support of “Mr. William H. Goodwin and Mrs. Alice Goodwin and the Commonwealth Foundation for Cancer Research”; NIH P41-EB015871–30 (J.W.K.); The Stanford Cancer Translational Nanotechnology Training Grant T32 CA196585 (R.M.D); U54 CA163004 (T.C.W.); George Will Foundation Berlin (S.R., C.H.C., S.S.G.); Kenneth Rainin Foundation for IBD research (S.H., S.R., and C.H.C.); and 1R01 CA182043–01A1 (C.H.C., S.S.G.). R.H. was supported in part by the National Natural Science Foundation of China 81771890. V.N. was supported by a DFG research fellowship grant no. NE1922/2–1. Part of this work was performed at the Stanford Nano Shared Facilities (SNSF), supported by the National Science Foundation under award ECCS-1542152. This research was funded in part through the MSKCC NIH/NCI Cancer Center Support Grant P30 CA008748.

REFERENCES

(1). Pennathur A; Landreneau RJ; Luketich JD Surgical Aspects of the Patient with High-Grade Dysplasia. Semin. Thorac. Cardiovasc. Surg 2005, 17, 326–332. [PubMed: 16428039]

(2). Selby JV; Friedman GD; Quesenberry CP, Jr.; Weiss NS A Case-Control Study of Screening Sigmoidoscopy and Mortality from Colorectal Cancer. N. Engl. J. Med 1992, 326, 653–657. [PubMed: 1736103]

(3). Winawer SJ; Zauber AG; Ho MN; O’Brien MJ; Gottlieb LS; Sternberg SS; Waye JD; Schapiro M; Bond JH; Panish JF; Ackroyd F; Shike M; Kurtz RC; Hornsby-Lewis L Prevention of Colorectal Cancer by Colonoscopic Polypectomy. The National Polyp Study Workgroup. N. Engl. J. Med 1993, 329, 1977–1981. [PubMed: 8247072]

(4). Siegel RL; Miller KD; Jemal A Cancer Statistics, 2016. Ca-Cancer J. Clin 2016, 66, 7–30. [PubMed: 26742998]

(5). Curvers WL; Bergman JJ Multimodality Imaging in Barrett’s Esophagus: Looking Longer, Seeing Better, and Recognizing More. Gastroenterology 2008, 135, 297–299. [PubMed: 18555016]

(6). Voutilainen ME; Juhola MT Evaluation of the Diagnostic Accuracy of Gastroscopy to Detect Gastric Tumours: Clinicopathological Features and Prognosis of Patients with Gastric Cancer Missed on Endoscopy. Eur. J. Gastroenterol. Hepatol 2005, 17, 1345–1349. [PubMed: 16292088]

(7). van Rijn JC; Reitsma JB; Stoker J; Bossuyt PM; van Deventer SJ; Dekker E Polyp Miss Rate Determined by Tandem Colonoscopy: A Systematic Review. Am. J. Gastroenterol 2006, 101, 343–350. [PubMed: 16454841]

(8). Wang YR; Cangemi JR; Loftus EV, Jr.; Picco MF Rate of Early/Missed Colorectal Cancers after Colonoscopy in Older Patients with or without Inflammatory Bowel Disease in the United States. Am. J. Gastroenterol 2013, 108, 444–449. [PubMed: 23295277]

(9). Solis-Munoz P; Solis-Herruzo JA; Lopez-Alonso G; Colina-Ruizdelgado F; Munoz-Yague T Unfound Gastric Signet Ring-Cell Adenocarcinoma after Gastric Biopsy. Endoscopy 2010, 42, 429−U25.

(10). Gupta M; Iyer PG; Lutzke L; Gorospe EC; Abrams JA; Falk GW; Ginsberg GG; Rustgi AK; Lightdale CJ; Wang TC; Fudman DI; Poneros JM; Wang KK Recurrence of Esophageal Intestinal Metaplasia after Endoscopic Mucosal Resection and Radiofrequency Ablation of Barrett’s Esophagus: Results from a US Multicenter Consortium. Gastroenterology 2013, 145, 79–86. [PubMed: 23499759]

(11). Vaccaro BJ; Gonzalez S; Poneros JM; Stevens PD; Capiak KM; Lightdale CJ; Abrams JA Detection of Intestinal Metaplasia after Successful Eradication of Barrett’s Esophagus with Radiofrequency Ablation. Dig. Dis. Sci 2011, 56, 1996–2000. [PubMed: 21468652]

(12). O’Connell MJ; Campbell ME; Goldberg RM; Grothey A; Seitz JF; Benedetti JK; Andre T; Haller DG; Sargent DJ Survival Following Recurrence in Stage II and III Colon Cancer: Findings from the ACCENT Data Set. J. Clin. Oncol 2008, 26, 2336–2341. [PubMed: 18467725]

(13). Lin D; Huang H; Qiu S; Feng S; Chen G; Chen R Diagnostic Potential of Polarized Surface Enhanced Raman Spectroscopy Technology for Colorectal Cancer Detection. Opt. Express 2016, 24, 2222–2234. [PubMed: 26906798]

(14). Wan QS; Wang T; Zhang KH Biomedical Optical Spectroscopy for the Early Diagnosis of Gastrointestinal Neoplasms. Tumor Biol 2017, 39, 1010428317717984.

(15). Harmsen S; Bedics MA; Wall MA; Huang R; Detty MR; Kircher MF Rational Design of a Chalcogenopyrylium-Based Surface-Enhanced Resonance Raman Scattering Nanoprobe with Attomolar Sensitivity. Nat. Commun 2015, 6, 6570. [PubMed: 25800697]

(16). Harmsen S; Huang R; Wall MA; Karabeber H; Samii JM; Spaliviero M; White JR; Monette S; O'Connor R; Pitter KL; Sastra SA; Saborowski M; Holland EC; Singer S; Olive KP; Lowe SW; Blasberg RG; Kircher MF Surface-Enhanced Resonance Raman Scattering Nanostars for High-Precision Cancer Imaging. Sci. Transl. Med 2015, 7, 271ra7.

(17). Huang R; Harmsen S; Samii JM; Karabeber H; Pitter KL; Holland EC; Kircher MF High Precision Imaging of Microscopic Spread of Glioblastoma with a Targeted Ultrasensitive SERRS Molecular Imaging Probe. Theranostics 2016, 6, 1075–1084. [PubMed: 27279902]

(18). Karabeber H; Huang R; Iacono P; Samii JM; Pitter K; Holland EC; Kircher MF Guiding Brain Tumor Resection Using Surface-Enhanced Raman Scattering Nanoparticles and a Hand-Held Raman Scanner. ACS Nano 2014, 8, 9755–9766. [PubMed: 25093240]

(19). Garai E; Sensarn S; Zavaleta CL; Loewke NO; Rogalla S; Mandella MJ; Felt SA; Friedland S; Liu JT; Gambhir SS; Contag CH A Real-Time Clinical Endoscopic System for Intraluminal, Multiplexed Imaging of Surface-Enhanced Raman Scattering Nanoparticles. PLoS One 2015, 10, e0123185. [PubMed: 25923788]

(20). Garai E; Sensarn S; Zavaleta CL; Van de Sompel D; Loewke NO; Mandella MJ; Gambhir SS; Contag CH High-Sensitivity, Real-Time, Ratiometric Imaging of Surface-Enhanced Raman Scattering Nanoparticles with a Clinically Translatable Raman Endoscope Device. J. Biomed. Opt 2013, 18, 096008. [PubMed: 24008818]

(21). Kircher MF; de la Zerda A; Jokerst JV; Zavaleta CL; Kempen PJ; Mittra E; Pitter K; Huang R; Campos C; Habte F; Sinclair R; Brennan C; Mellinghoff IK; Holland EC; Gambhir SS A Brain Tumor Molecular Imaging Strategy Using a New Triple-Modality MRI-Photoacoustic-Raman Nanoparticle. Nat. Med 2012, 18, 829–34. [PubMed: 22504484]

(22). Quante M; Bhagat G; Abrams JA; Marache F; Good P; Lee MD; Lee Y; Friedman R; Asfaha S; Dubeykovskaya Z; Mahmood U; Figueiredo JL; Kitajewski J; Shawber C; Lightdale CJ; Rustgi AK; Wang TC Bile Acid and Inflammation Activate Gastric Cardia Stem Cells in a Mouse Model of Barrett-Like Metaplasia. Cancer Cell 2012, 21, 36–51. [PubMed: 22264787]

(23). Spechler SJ; Souza RF Barrett's Esophagus. N. Engl. J. Med 2014, 371, 836–845. [PubMed: 25162890]

(24). Castella E; Ariza A; Fernandez-Vasalo A; Roca X; Ojanguren I Expression of CD44H and CD44v3 in Normal Oesophagus, Barrett Mucosa and Oesophageal Carcinoma. J. Clin. Pathol 1996, 49, 489–492. [PubMed: 8763264]

(25). Tomita H; Takaishi S; Menheniott TR; Yang X; Shibata W; Jin G; Betz KS; Kawakami K; Minamoto T; Tomasetto C; Rio MC; Lerkowit N; Varro A; Giraud AS; Wang TC Inhibition of Gastric Carcinogenesis by the Hormone Gastrin is Mediated by Suppression of TFF1 Epigenetic Silencing. Gastroenterology 2011, 140, 879–891. [PubMed: 21111741]

(26). Moser AR; Luongo C; Gould KA; McNeley MK; Shoemaker AR; Dove WF ApcMin: A Mouse Model for Intestinal and Mammary Tumorigenesis. Eur. J. Cancer 1995, 31A, 1061–1064. [PubMed: 7576992]

(27). Hulit J; Wang C; Li Z; Albanese C; Rao M; Di Vizio D; Shah S; Byers SW; Mahmood R; Augenlicht LH; Russell R; Pestell RG Cyclin D1 Genetic Heterozygosity Regulates Colonic Epithelial Cell Differentiation and Tumor Number in ApcMin Mice. Mol. Cell. Biol 2004, 24, 7598–7611. [PubMed: 15314168]

(28). Moser AR; Mattes EM; Dove WF; Lindstrom MJ; Haag JD; Gould MN ApcMin, a Mutation in the Murine Apc Gene, Predisposes to Mammary Carcinomas and Focal Alveolar Hyperplasias. Proc. Natl. Acad. Sci. U. S. A 1993, 90, 8977–8981. [PubMed: 8415640]

(29). Powell SM; Petersen GM; Krush AJ; Booker S; Jen J; Giardiello FM; Hamilton SR; Vogelstein B; Kinzler KW Molecular Diagnosis of Familial Adenomatous Polyposis. N. Engl. J. Med 1993, 329, 1982–1987. [PubMed: 8247073]

(30). Powell SM; Zilz N; Beazer-Barclay Y; Bryan TM; Hamilton SR; Thibodeau SN; Vogelstein B; Kinzler KW APC Mutations Occur Early During Colorectal Tumorigenesis. Nature 1992, 359, 235–237. [PubMed: 1528264]

(31). Maeda H Tumor-Selective Delivery of Macromolecular Drugs via the EPR Effect: Background and Future Prospects. Bioconjugate Chem 2010, 21, 797–802.

(32). Maeda H; Tsukigawa K; Fang J A Retrospective 30 Years After Discovery of the Enhanced Permeability and Retention Effect of Solid Tumors: Next-Generation Chemotherapeutics and Photodynamic Therapy–Problems, Solutions, and Prospects. Microcirculation 2016, 23, 173–182. [PubMed: 26237291]

(33). Hagendoorn J; Tong R; Fukumura D; Lin Q; Lobo J; Padera TP; Xu L; Kucherlapati R; Jain RK Onset of Abnormal Blood and Lymphatic Vessel Function and Interstitial Hypertension in Early Stages of Carcinogenesis. Cancer Res 2006, 66, 3360–3364. [PubMed: 16585153]

(34). James ML; Gambhir SS A Molecular Imaging Primer: Modalities, Imaging Agents, and Applications. Physiol. Rev 2012, 92, 897–965. [PubMed: 22535898]

(35). Kim YI; Jeong S; Jung KO; Song MG; Lee CH; Chung SJ; Park JY; Cha MG; Lee SG; Jun BH; Lee YS; Hwang DW; Youn H; Kang KW; Lee YS; Jeong DH; Lee DS Simultaneous Detection of EGFR and VEGF in Colorectal Cancer using Fluorescence-Raman Endoscopy. Sci. Rep 2017, 7, 1035. [PubMed: 28432289]

(36). Wang YW; Kang S; Khan A; Bao PQ; Liu JT C. In Vivo Multiplexed Molecular Imaging of Esophageal Cancer via Spectral Endoscopy of Topically Applied SERS Nanoparticles. Biomed. Opt. Express 2015, 6, 3714–3723. [PubMed: 26504623]

(37). Beerenwinkel N; Antal T; Dingli D; Traulsen A; Kinzler KW; Velculescu VE; Vogelstein B; Nowak MA Genetic Progression and the Waiting Time to Cancer. PLoS Comput. Biol 2007, 3, e225. [PubMed: 17997597]

(38). Ahlquist DA; Zou H; Domanico M; Mahoney DW; Yab TC; Taylor WR; Butz ML; Thibodeau SN; Rabeneck L; Paszat LF; Kinzler KW; Vogelstein B; Bjerregaard NC; Laurberg S; Sorensen HT; Berger BM; Lidgard GP Next-generation Stool DNA Test Accurately Detects Colorectal Cancer and Large Adenomas. Gastroenterology 2012, 142, 248–56. [PubMed: 22062357]

(39). Traverso G; Shuber A; Levin B; Johnson C; Olsson L; Schoetz DJ, Jr.; Hamilton SR; Boynton K; Kinzler KW; Vogelstein B Detection of APC Mutations in Fecal DNA from Patients with Colorectal Tumors. N. Engl. J. Med 2002, 346, 311–320. [PubMed: 11821507]

(40). Libutti SK; Paciotti GF; Byrnes AA; Alexander HR, Jr.; Gannon WE; Walker M; Seidel GD; Yuldasheva N; Tamarkin L Phase I and Pharmacokinetic Studies of CYT-6091, a Novel PEGylated Colloidal Gold-rhTNF Nanomedicine. Clin. Cancer Res 2010, 16, 6139–6149. [PubMed: 20876255]

(41). Stern JM; Solomonov VVK; Sazykina E; Schwartz JA; Gad SC; Goodrich GP Initial Evaluation of the Safety of Nanoshell-Directed Photothermal Therapy in the Treatment of Prostate Disease. Int. J. Toxicol 2016, 35, 38–46. [PubMed: 26296672]

(42). Harmsen S; Wall MA; Huang R; Kircher MF Cancer Imaging Using Surface-Enhanced Resonance Raman Scattering Nanoparticles. Nat. Protoc 2017, 12, 1400–1414. [PubMed: 28686581]

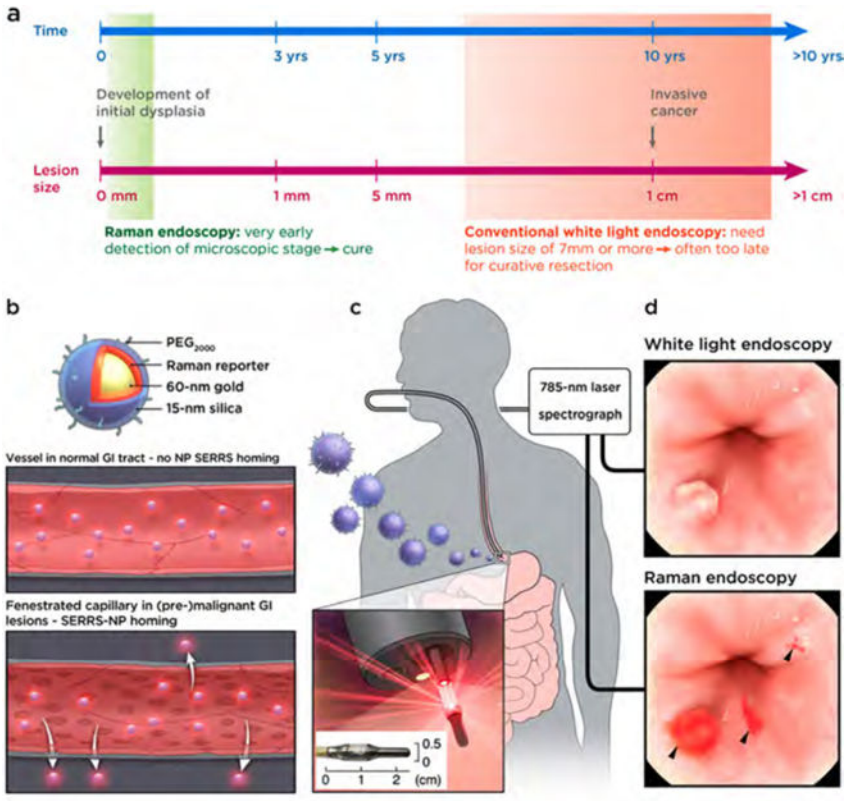

Figure 1.

Concept of contrast-enhanced Raman imaging of gastrointestinal lesions. In contrast to white-light endoscopy, very small premalignant lesions, microscopic malignant lesions, and otherwise occult (flat) lesions can be detected. (a) Comparison of lesion detectability between SERRS-NP-enhanced Raman endoscopy and conventional white-light endoscopy currently used in the clinic. While white-light endoscopy requires lesions to be at least 5−7 mm in size to be detectable, Raman endoscopy can detect lesions at 0.5−1.0 mm. Depending on the growth characteristics of different GI tumors, Raman endoscopy has the potential to "catch" lesions much earlier, at a premalignant stage where localized lesion removal could result in cures (depicted time line is approximated for colon cancer; there are large variations, and other GI tumors can grow much faster). (b) Rendered cross-section diagram of the SERRS-NPs used. (c) Envisioned clinical use: intravenously injected SERRS-NPs specifically accumulate in (pre-) malignant lesions. Given the very high sensitivity of detecting the SERRS-NPs and their specific accumulation *via* the EPR effect, specific targeting moieties are not required. Thus, this approach may be a universal detection strategy for (pre-) malignant GI tract lesions. Raman-scattered photons are recorded by the Raman endoscope with a rotating mirror, enabling it to acquire two two-dimenstional images of the GI tract lumen: a Raman image that is superimposed on the surface topology of the luminal surface. Inset: The distal end of the circumferentially scanning Raman endoscope includes a rotating mirror that distributes the laser circumferentially along the luminal surface of the colon. As the Raman endoscope is designed to fit into the instrument channel of a clinical white-light endoscope currently used in the clinic, concomitant dual-modal white-light/ Raman imaging can be acquired in the same endoscopic session. Data are analyzed and

collected by the spectrograph and CCD image sensor, respectively. (d) Illustration of the acquired imaging data. The traditional white-light endoscope can visualize polypoid lesions above a certain size (usually a size of >5−7 mm is required). However, the Raman signals from the SERRS-NP fingerprint enable detection of much smaller lesions. Of note, the SERRS detection does not depend on the lesion morphology or molecular markers, so that even flat lesions (usually missed with conventional white-light endoscopy) can be visualized. This graphic was created by the MSKCC Graphic Department, and permission for use obtained.

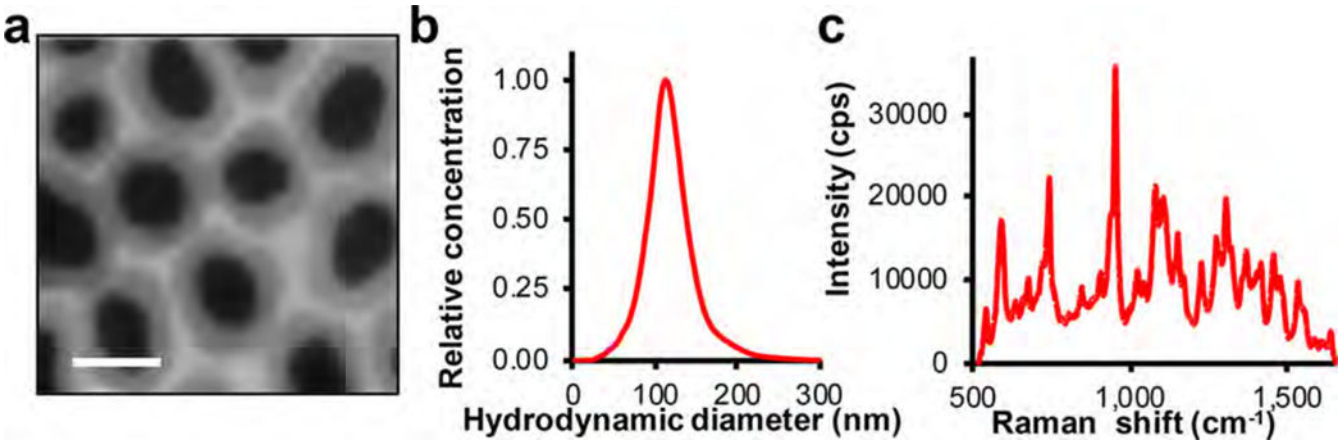

Figure 2.

PEGylated SERRS-NP characterization. (a) Transmission electron micrograph of SERRS-NPs at a magnification of 100,000×. Scale bar: 100 nm. (b) Hydrodynamic diameter of PEGylated SERRS-NPs in water as determined by nanoparticle tracking analysis. (c) Fingerprint-like surface-enhanced resonance Raman spectrum of 785 nm laser (50 μW; 1.0 s) excited PEGylated SERRS-NPs (10 μL; 1.0 nM in water).

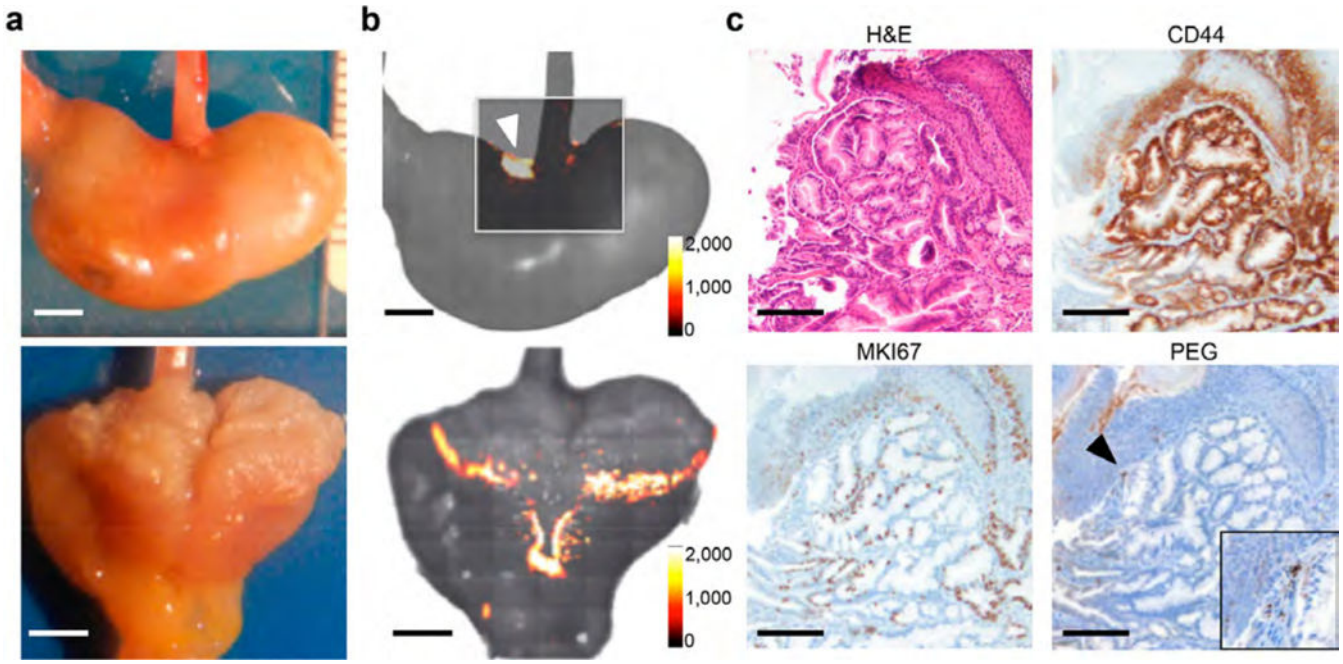

Figure 3.

Early detection of lesions at the gastroesophageal junction (GEJ) by SERRS-based Raman imaging. (a) Photograph of a closed mouse stomach (upper row) and a stomach opened along the greater curvature (lower row) of bile-acid-treated *L2-hIL-1β* mice tail-vein injected with 30 fmol/g SERRS-NPs (scale bar, 2 mm). (b) *Ex vivo* Raman imaging demonstrated SERRS-positive lesions at the GEJ (white arrowhead; intensity of the diagnostic 950 cm^{-1} Raman band in counts per second). SERRS-positive lesions were found at the GEJ and along the gastric cardia (intensity of the diagnostic 950 cm^{-1} Raman band in counts per second; scale bar, 2 mm) in the opened stomach (lower row); the Raman positive pattern fits the locations of dysplasia commonly seen by histological examination in this model of Barrett's esophagus. (c) Histologic examination of the SERRS-positive region (arrowhead in b) at the GEJ was graded as dysplastic by a veterinary pathologist. The positive anti-PEG stain further confirms the presence of the SERRS-NPs in the indicated lesion (scale bars, 100 μm). The inset shows a higher magnification (4×) of the granular PEG staining in the focus indicated by the black arrowhead.

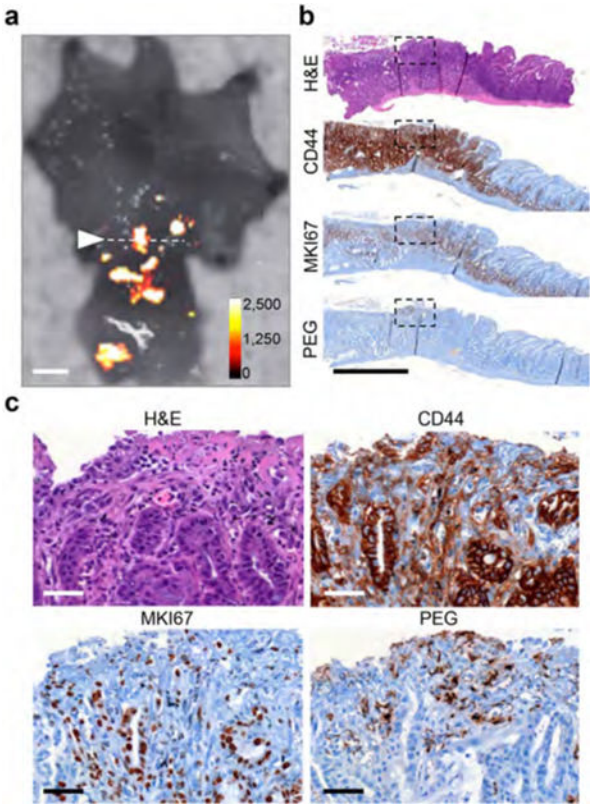

Figure 4.

Detection by SERRS-based Raman imaging of gastric dysplasia at the pyloric antrum of *Helicobacter felis*-infected/MNU-treated GAS-KO mouse. (a) The stomach of an *H. felis*/MNU-treated GAS-KO mouse injected with SERRS-NPs was opened along the greater curvature and scanned by Raman imaging (intensity in counts per second). SERRS-positive lesions were detected at the pyloric antrum. The dotted line shows the location along which a SERRS-positive lesion was sectioned transversely (scale bar, 2 mm). (b) Overview (scale bar, 1 mm) and (c) higher magnification (20×) views of the immunohistochemical sections (dotted box) that were stained for CD44, MKI67, and polyethylene glycol (PEG; polymer on the surface of the SERRS nanoparticle; scale bar, 50 μm). While in a normal stomach CD44 would be confined to the lower glandular cells of the pyloric antrum, here CD44 is diffusely expressed in the SERRS-positive lesion. The diffuse coexpression of MKI67 along with the abnormal morphology seen on H&E is indicative of dysplasia. See also Supplementary Figure S4.

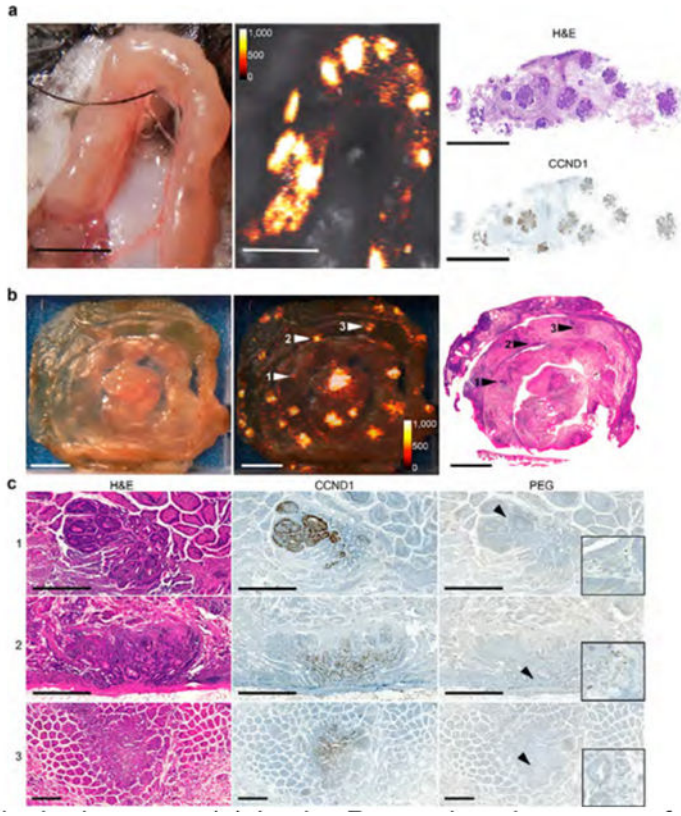

Figure 5.

SERRS NP-mediated detection of intestinal adenomas. *(a) In vivo* Raman imaging was performed on an exteriorized bowel loop in an isoflurane-anesthetized $Apc^{Min/+}$ mouse. Raman imaging identified multiple SERRS-positive lesions (middle panel; SERRS signal in counts per second) that all corresponded to adenomas as confirmed by histology (right panel; H&E staining and CCND1 immunohistochemistry). All scale bars: 5 mm. (b) To determine the sensitivity of SERRS-based Raman imaging for (pre-) malignant lesion detection, segments of the small intestine of $Apc^{Min/+}$ mice ($n = 4$) injected with SERRS-NPs were scanned by Raman imaging *ex vivo* (middle panel; intensity in counts per second; scale bars, 5 mm). Even lesions less than 1 mm were detected by Raman imaging and would have been missed by macroscopic observation. The tissues were sectioned, and the 5 μm tissue sections were stained with H&E (right panel) and for CCND1 and PEG, respectively. (c) SERRS-positive lesions were correlated to histologic appearance and CCND1 status. As shown for the lesions indicated by arrowheads 1−3 in panel (b), SERRS signal correlates to the presence of dysplastic lesions. α-PEG was used to corroborate the presence of the SERRS-NPs (all scale bars, 500 μm; insets show 16× magnifications of the areas indicated by the arrow heads). See also Table 1 and Supplementary Figures S5−S7.

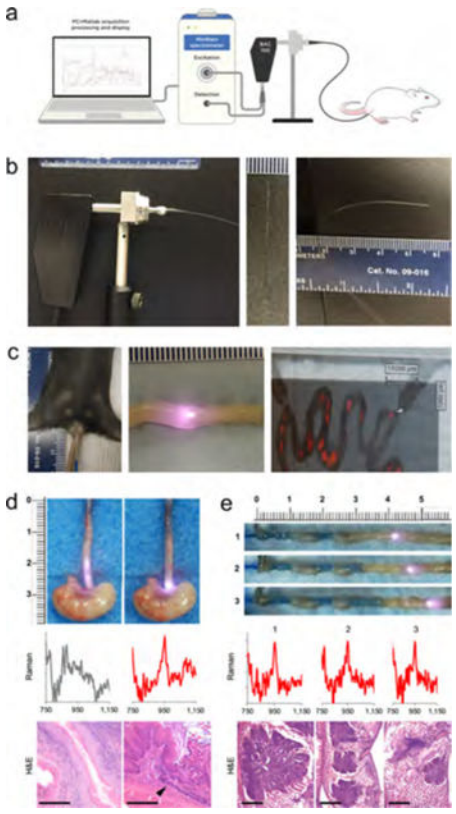

Figure 6.

Custom-built mouse Raman endoscope and testing in upper and lower GI tract models. (a) Diagram of mouse endoscope system. (b) Images of the custom-built mouse Raman fiberscope. The metallic shaft lens housing of a B&W BAC100 unit was replaced with a multimode optical fiber (Ⓘ 550 μm) and connected to a B&WTek MiniRam Raman spectrometer. (c) Endoscope inserted into the colon of a live $Apc^{Min/+}$ mouse (left). Image of an endoscope inserted into an exteriorized intestinal segment of the colon of an $Apc^{Min/+}$ mouse with the laser activated (middle). SERRS-NP signal was detected at this location. Image of exteriorized intestinal loops imaged with the InVia System (right). Shown is a Raman/white-light overlay, with the white arrow indicating the location of a Raman-positive lesion that was detected with the endoscope. Endoscopy was performed with a 785 nm diode laser operating at 50 mW laser power using an acquisition time of 100 ms. (d) The GI tract was surveyed *ex vivo* with the endoscope. The endoscope was descended along the esophagus. A Raman spectrum was collected 8 mm proximal of the GEJ (gray) and at the GEJ (red). As shown, the spectral fingerprint of the SERRS-NP (950 cm^{-1} band) was only found at the GEJ (red). While the tissue architecture in the longitudinal section of the proximal GEJ appears normal with only mild to moderate diffuse infiltrate of lymphocytes, plasma cells, and neutrophils within the lamina propria and submucosa, histopathological examination confirmed the presence of disease in a transverse section of the GEJ (arrowhead) sectioned from the same animal. There is focal metaplasia of the epithelium, with abrupt transition from stratified squamous to simple columnar with goblet cell differentiation (intestinal metaplasia). There is erosion of the superficial mucosal epithelium within and immediately adjacent to the focus of metaplasia. Scale bar: 200 μm. (e) The

Raman endoscope was carefully inserted into the small intestine proximally to the cecum and slowly advanced along the small intestine. When SERRS-NP signal was detected, the tissue was resected (1−3) and processed for histologic examination (H&E; scale bar, 1 mm).

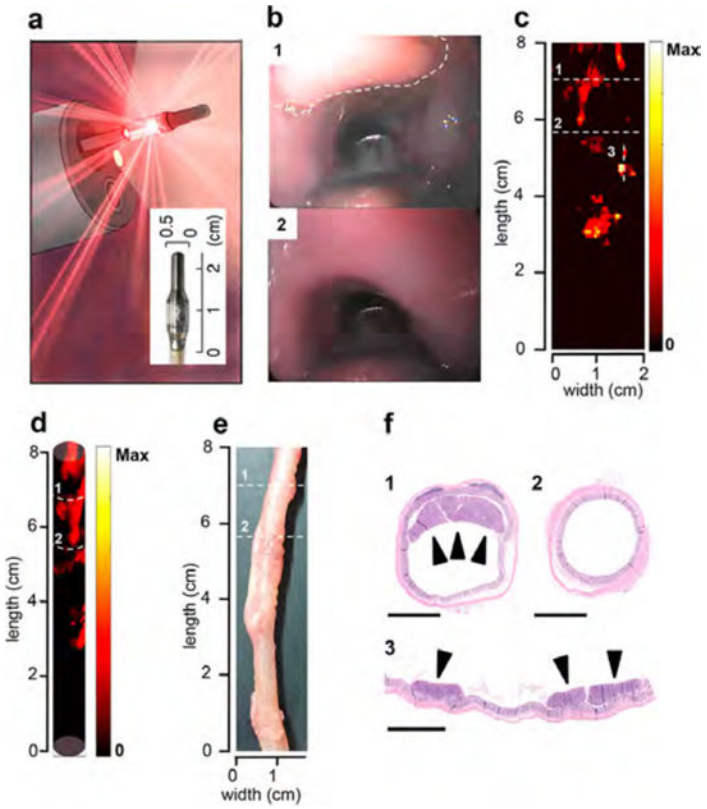

Figure 7.

SERRS-NP-augmented endoscopic Raman imaging of premalignant colorectal lesions using the clinical Raman/white light endoscope. (a) Schematic rendering of the clinical Raman endoscope inserted into the accessory channel of a conventional clinical white-light endoscope. Inset: Photograph of the tip of the Raman endoscope. (b) White-light endoscopic imaging of polyp ("1"; dashed line) and normal tissue ("2") in the colon of an $Apc^{Pirc/+}$ rat. (c) 2D representation of the SERRS-NP-generated signal intensity along the length of the colon of the same $Apc^{Pirc/+}$ rat. The colon was sectioned along the dashed lines. (d) 3D cylindrical projection of the 2D Raman map (also see Supplemental Movie 1). (e) *Ex vivo* white-light image of the examined colon. (f) The SERRS signal correlated with the presence of an adenomatous polyp(s) ("1" and "3"), while no lesions were found in the SERRS-negative section ("2"). All scale bars: 2.5 mm.

Table 1.

Sensitivity and Precision of SERRS-Based Raman Imaging for Adenoma Detection

sample	total SERRS positive	total lesions (H&E)	true positive	false positive	false negative	sensitivity	positive predictive value
#1	27	19	16 (16/19)	3 (3/19)	0 (0/19)		
#2	52	30	27 (27/30)	1 (1/30)	2 (2/30)		
#3	20	16	15 (15/16)	1 (1/16)	0 (0/16)		
#4	35	27	24 (24/27)	1 (1/27)	2 (2/27)		
total	134	92	82 (82/92)	6 (6/92)	4 (4/92)	93.1%	89% (95% CI)